ACS APPLIED MATERIALS & INTERFACES

Research Article

www.acsami.org

Targeted Near-Infrared Fluorescent Turn-on Nanoprobe for Activatable Imaging and Effective Phototherapy of Cancer Cells

Na Li, Tingting Li, Chao Hu, Xiaomin Lei, Yunpeng Zuo, and Heyou Han*

State Key Laboratory of Agricultural Microbiology, College of Science, College of Food Science and Technology, Huazhong Agricultural University, Wuhan 430070, P. R. China

Supporting Information

ABSTRACT: A novel and green multifunctional nanoplatform as a nanocarrier for drug delivery, cell imaging, and phototherapy has been engineered. The nanoplatform is composed of stabilized carbon spheres (CSs) as cores, a coated polydopamine (PDA) shell, targeted folic acid (FA), and the loaded anticancer drug indocyanine green (ICG), obtaining CSs@PDA-FA@ICG nanocomposites (NCs). The biocompatible PDA shell provided a high fluorescence quenching efficiency and a surface rich in functional groups for anchoring FA for targeting cancer cells. Aromatic ICG could be effectively loaded into the CSs@PDA-FA system via hydrophobic interactions and $\pi-\pi$ stacking with a loading efficiency of 58.9%. Notably, the activated NIR fluorescence in an intracellular environment made CSs@PDA-FA@ICG a sensitive "OFF" to "ON" nanoprobe that can be used for NIR imaging. Moreover, compared to ICG alone, the CSs@PDA-FA@ICG NCs could induce efficient photoconversion for simultaneous synergetic photodynamic therapy (PDT) and photothermal therapy (PTT) under a single NIR laser irradiation. The results demonstrated that CSs@PDA-FA@ICG NCs as a targeted and activated nanoplatform provide new opportunities to facilitate the accurate diagnosis of cancer and enhanced treatment efficacy. This work stimulates more interest in the design of the facile surface functionalization strategy to construct other multifunctional nanocomposites, such as nanotubes and nanorods.

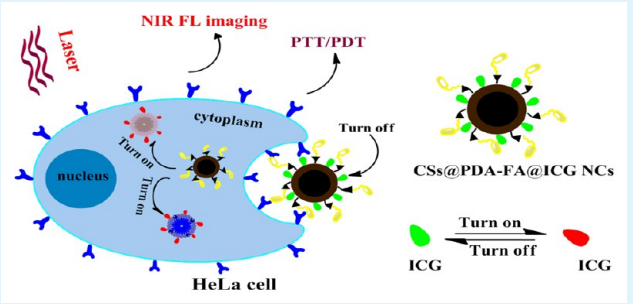

KEYWORDS: *multifunctional nanocomposites, fluorescence quenching, turn-on, NIR imaging, phototherapy*

1. INTRODUCTION

The early diagnosis and therapy of cancer cells for increasing cancer patient survival rate is still a great challenge. An efficient theranostic platform for cancer requires the integration of imaging, targeting, and multimodality therapy in a single system.[1−3] Recently, the graphene and carbon tube, as members of the carbon family, have been widely applied in the preparation of multifunctional nanocomposites (NCs) for biomedical applications.[4,5] However, there have been few reports discussing surface modification of carbon spheres for biomedical applications. Carbon spheres, as one of the sp^2 carbon nanomaterials, has attracted a great deal of research interest in biological applications because of their easy synthesis and unique intrinsic physical and chemical properties.[6−8] For example, Liu et al.[9] reported the preparation of surface engineered carbon nanospheres with high drug loading efficiency for pH responsive delivery of doxorubicin to cancer cells. Therefore, the carbon spheres can be used as carriers for biomedical applications. Moreover, they can serve as efficient photosensitizers with high absorption in the near-infrared (NIR) region and high-thermal stability for photothermal therapy.[10−12] Recently, several research groups have successfully constructed the multifunctional nanoplatform based on carbon sphere nanoparticles for imaging and thermo-chemotherapy of cancer.[9−12] Therefore, carbon spheres (CSs) can be exploited for biomedical applications, such as photothermal therapy and drug delivery. In addition, we expect that CSs can not only possess ordinary properties and functions but also have the capability of targeting recognition or diagnosis and be sensitive to intracellular stimuli to release drugs. Hence, dopamine (DA) is used to accomplish the multifunctionalization and biocompatibility of CSs. DA can self-polymerize at alkaline pH values, and the generated polydopamine (PDA) can spontaneously deposit on the surface of CSs.[13] The PDA possesses unique physicochemical properties and excellent biocompatibility. It is reported that PDA can serve as a universal coating for nanoparticles (e.g., gold nanorods, magnetic nanoparticles, and carbon nanotubes) for various applications,[13−15] including surface modification, metal deposition, and drug delivery (directly adsorbing anticancer drugs by $\pi-\pi$ interactions). Therefore, PDA-coated CSs (CSs@PDA) as a novel nanoplatform is highly desired to optimize photophysical performance as well as enhance bioactivity and promote cell proliferation of the CSs.[15−17] Furthermore, the existence of functional groups (amine) on the surface of PDA can be modified with various biomolecules (for example, folic

Received: March 7, 2015
Accepted: May 21, 2015
Published: May 21, 2015

DOI: 10.1021/acsami.5b02037
ACS Appl. Mater. Interfaces 2016, 8, 15013−15023

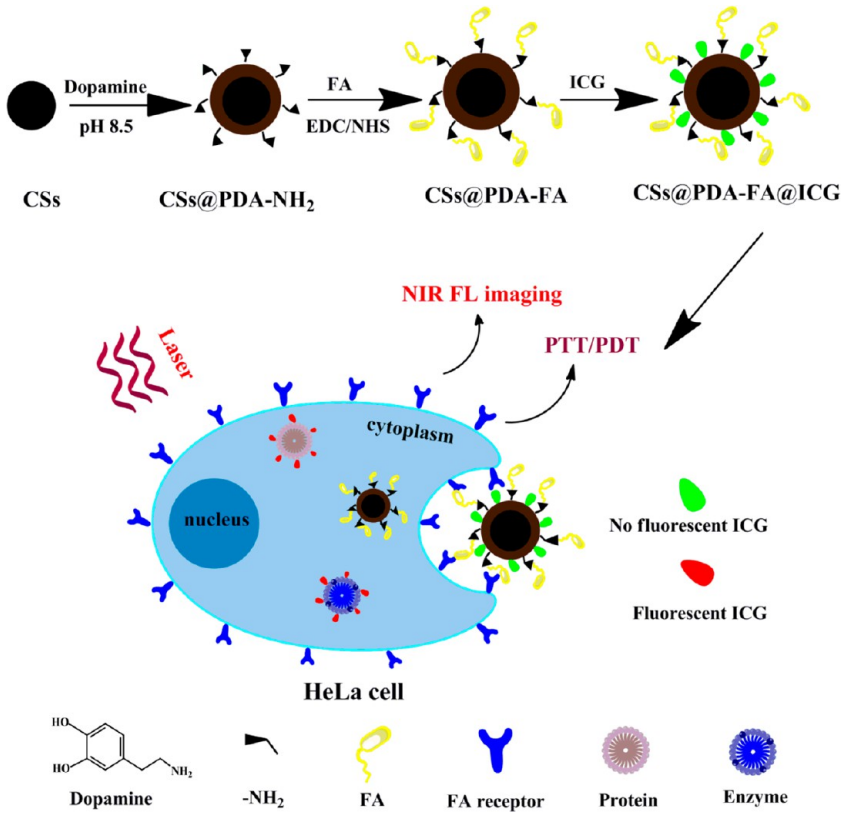

Figure 1. Schematic illustration of the preparation of CSs@PDA-FA@ICG NCs and their application for targeted, activation-capable imaging and phototherapy of cancer cells.

acid (FA)). The FA-modified CSs@PDA (CSs@PDA-FA) makes it have a high selectivity and binding affinity to the folate receptor that is overexpressed on cancer cell surfaces.[18,19] These days, PDA is also being used as a phototherapeutic agent for cancer therapy due to its strong NIR absorption and high photothermal conversion efficiency (40%).[13,17] Considering these features, we inferred that the targeted CSs@PDA-FA nanoparticles would be a very suitable material in the preparation of nanocomposites for biomedical applications.

To realize effective diagnosis and treatment of cancer cells, the loading of various fluorescent anticancer drugs on the surface of CSs@PDA-FA is significant for constructing multifunctional nanocomposites for theranostic applications. Indocyanine green (ICG) with NIR absorption and emission for effective photothermal/photodynamic response has been applied for NIR imaging and phototherapy. In particular, ICG as a novel NIR photoactivating probe in biomedical studies has good foreground because of their tissue penetration, low autofluorescence, and minimal tissue injury.[20−22] However, the practical applications of ICG in PTT/PDT and NIR imaging are restricted due to their poor aqueous stability, unstable optical properties, quick degradation, and clearance in the living body.[23] Therefore, there is great need to propose a safe and effective method for facilitating the delivery of ICG drugs for an enhanced penetration and retention (EPR) effect and fluorescence stability for NIR imaging and therapy. Recently, several research groups have proposed some targeting ICG nanocarriers, such as polyallylamine, calcium phosphosilicate, and perfluorocarbon, which can be used for improving stability and targeted imaging.[24−26] However, it is still urgent to develop a facile and activatable targeting ICG nanocarrier for the efficient imaging and therapy of cancer cells. Here, the CSs@PDA-FA has the capacity to adsorb and load ICG aroused by the weak $\pi-\pi$ stacking interaction.[13,27−29] Furthermore, the coated PDA shell can effectively quench the fluorescence of the ICG dye. Therefore, the loaded ICG in CSs@PDA-FA is in the fluorescence "OFF" state. After the CSs@PDA-FA@ICG NC is taken up by targeted cancer cells, the ICG is gradually released from the NCs, which induces the activation of ICG fluorescence to the "ON" state. This is because ICG highly bonded to intracellular protein (e.g., glutathione S-transferase) distributed in the cytoplasm results in ICG fluorescent turn-on.[30,31] The NIR fluorescence of CSs@PDA-FA@ICG NCs could be activated (high signal) in the intracellular environment whereas a low fluorescence signal is detected (low noise) in a nonstimulating environment. Thus, it is very significant to fabricate a CSs@PDA-FA@ICG nanoplatform to generate a high signal-to-noise ratio (S/N ratio) for effective imaging and sensitive detection of cancer cells. Moreover, the nanoplatform can integrate PDT and PTT in a system. Over all, the development of a multifunctional fluorescent turn-on nanoplatform is very important for the detection and targeted therapy of cancer cells.

In this work, we constructed multifunctional CSs@PDA-FA@ICG NCs that can be utilized for the detection and phototherapy of cancer cells. To the best of our knowledge, no NIR fluorescence-based turn-on CSs@PDA-FA@ICG nanoprobes for activatable imaging and effective phototherapy of cancer cells have been explored to date. Herein, the modification of green CSs with biocompatible PDA (CSs@PDA) was achieved by in situ polymerization of DA onto the surface of the CSs (Figure 1). Next, FA was functionalized on the surface of CSs@PDA by covalent coupling, obtaining CSs@PDA-FA for enhancing the cellular uptake. Furthermore, we

DOI: 10.1021/acsami.5b02037
ACS Appl. Mater. Interfaces 2016, 8, 15013−15023

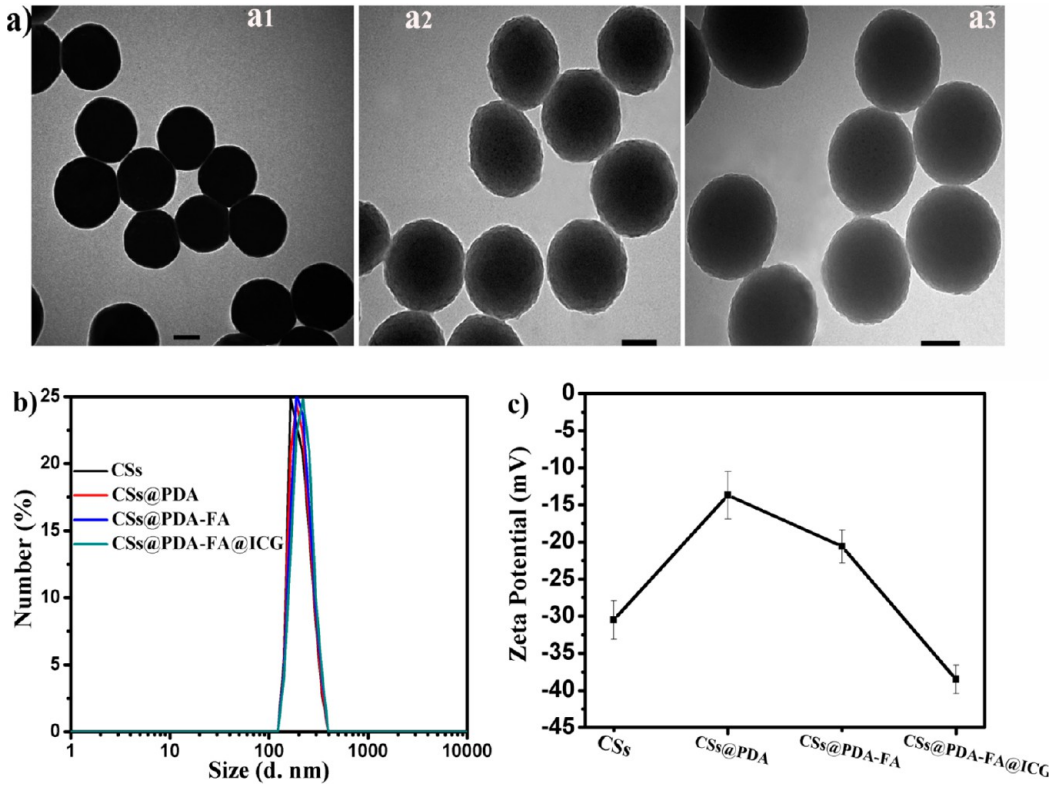

Figure 2. (a) TEM images of the CSs (a_1), CSs@PDA (a_2), and CSs@PDA-FA@ICG NCs (a_3); bar = 100 nm. (b) Size distribution of CSs, CSs@PDA, CSs@PDA-FA, and CSs@PDA-FA@ICG. (c) The zeta potential of CSs, CSs@PDA, CSs@PDA-FA, and CSs@PDA-FA@ICG.

demonstrated that CSs@PDA-FA can strongly adsorb ICG dye and effectively quench the fluorescence of ICG, but the strong binding between ICG and the intracellular proteins would result in the release of ICG from the nanocomposite and subsequent recovery of fluorescence. Therefore, a novel approach based on fluorescent turn-on is proposed for the activated NIR imaging of cancer cells. Moreover, the NCs can enhance phototherapy efficiency due to integration of the photoconversion performance of CSs, PDA, and ICG in a single system. Our results demonstrate that the engineered CSs@PDA-FA can serve as an ICG carrier and quencher to manipulate targeted and activated imaging; the synergetic PTT/PDT can efficiently kill target cancer cells under a single NIR laser irradiation.

2. EXPERIMENTAL SECTION

2.1. Materials. Cetyltrimethylammonium bromide (CTAB), *N*-hydroxy-sulfosuccin-imide (sulfo-NHS), 1-ethyl-3-(3-dimethylamino-propyl) carbodiimide hydrochloride (EDC), 2′,7′-dichlorofluorescin diacetate (DCFH-DA), indocyanine green (ICG), and 3-(4, 5-dimethyl-thiazol-2-yl)-2,5-diphenyltetrazolium bromide (MTT) were purchased from Sigma-Aldrich. Folic acid (FA) was purchased from Aladdin. Glucose and sodium azide (NaN_3) were purchased from Sinopharm Chemical Reagent Co. All cells were obtained from State Key Laboratory of Agricultural Microbiology. Ultrapure water with a conductivity of 18.25 MΩ cm was used throughout the experiments.

2.2. Apparatus and Characterization. The freshly purified CSs, CSs@PDA, and CSs@PDA-FA@ICG solution were transferred onto a 200 mesh copper grid coated with carbon, dried at room temperature, then analyzed by a JEM-2010FEF transmission electron microscope (TEM) at an accelerating voltage of 100 kV. The size and zeta potential of the nanoparticles (at a concentration of 0.05 mg mL^{-1}) were measured by dynamic light scattering (DLS) using a Malvern Zeta Sizer (Nano-ZS). The samples were first purified by repeated centrifugation at 13000 rpm for 4 min. Before the measurement, the nanoparticles were completely redispersed in PBS (0.01 M, pH 7.5) by ultrasonication for a modest amount of time. Multiple runs (>3) were performed to avoid erroneous results. The ultraviolet−visible (UV−Vis) absorption spectra were measured by a Nicolet Evolution 300 UltravioletVisible spectrometer. The Fluorescence spectra were recorded by an Edinburgh FLS920 spectrometer. The cell imaging was obtained with a Nikon inverted CMS DM-4000 M fluorescence microscope. A CW diode laser with a wavelength of 808 nm was used for the laser irradiation experiment.

2.3. Preparation of CSs. Glucose (4.0 g) and CTAB (0.30 g) were dissolved in ultrapure water (40 mL). The solution was transferred to a Teflon-lined stainless steel autoclave with a capacity of 100 mL. The autoclave was heated at 180 °C for 3 h and then cooled to room temperature. After being cooled to room temperature, the obtained CSs were repeatedly washed with water and ethanol at least ten times with centrifugation at 13000 rpm for 4 min and then redispersed in ultrapure water.

2.4. Synthesis of CSs@PDA. Eight milligrams of dopamine was added to 20 mL of a 1.0 mg mL^{-1} CS solution. Tris-base was added, and the pH was adjusted to 8.5. After shaking at room temperature for 12 h, CSs@PDA was obtained by centrifugation and washed with water several times.

2.5. Preparation of CSs@PDA-FA@ICG NCs. Ten milligrams of FA, 4.0 mg of EDC, and 4.0 mg of sulfo-NHS were mixed in 1.0 mL of DMSO. The FA was activated for 2 h at 25 °C. Then, 10 mL of 1.0 mg mL^{-1} of CSs@PDAs was added and stirred for 2 h. The obtained CSs@PDA-FA was purified. Next, ICG (1.0 mg) in 1.0 mL of PBS (pH 7.4) was mixed with CSs@PDA-FA (1.0 mg mL^{-1}) at 25 °C for 2 h, producing CSs@PDA-FA@ICG NCs.

2.6. Cytotoxicity Assay. The in vitro cytotoxicity was measured by MTT assay.[32] HeLa cells and normal hepatocytes (1×10^5 cells/well) were respectively seeded into 96-well cell culture plates and then incubated for 24 h at 37 °C under 5% CO_2. Then, the various concentrations of CSs, CSs@PDA-FA, free ICG, and CSs@PDA-FA@ICG NCs were respectively added and incubated for another 24 or 48

DOI: 10.1021/acsami.5b02037
ACS Appl. Mater. Interfaces 2016, 8, 15013−15023

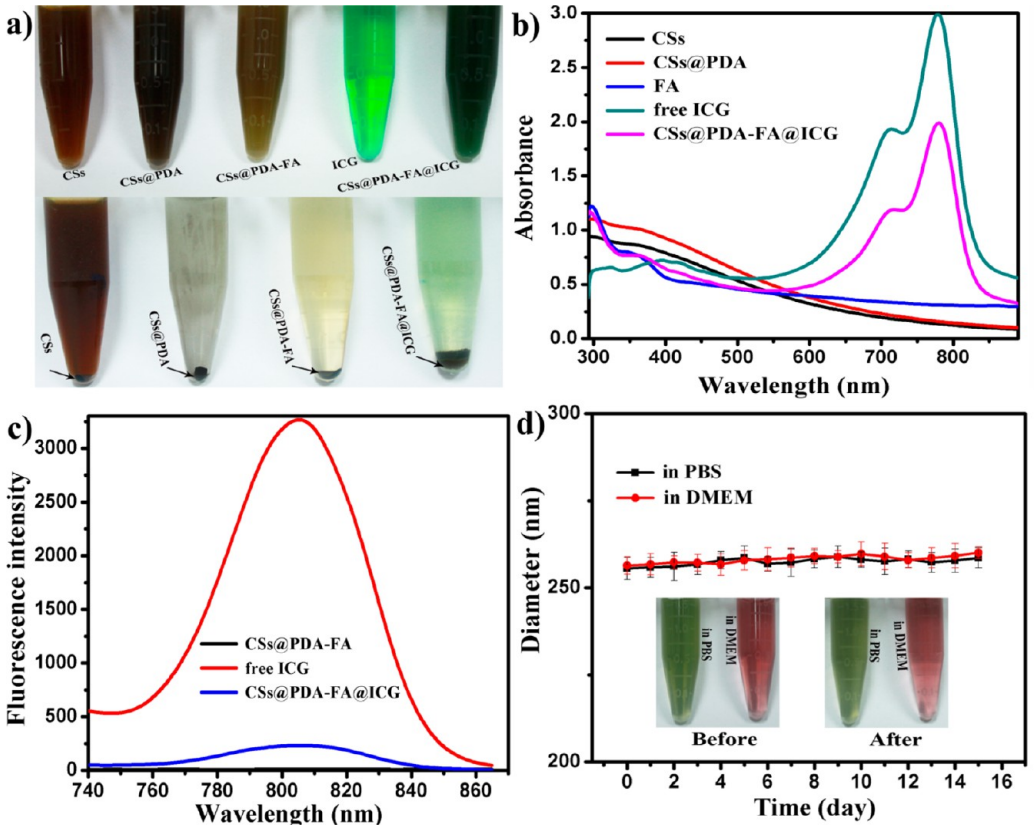

Figure 3. (a) (top) Color change of CSs, CSs@PDA, CSs@PDA-FA, ICG, and CSs@PDA-FA@ICG solutions in PBS; (bottom) precipitates of CSs, CSs@PDA, CSs@PDA-FA, and CSs@PDA-FA@ICG. (b) UV−vis absorption spectra of CSs, CSs@PDA, FA, free ICG, and CSs@PDA-FA@ICG solutions (0.05 mg mL^{-1}). (c) NIR fluorescence emission spectra of CSs@PDA-FA, free ICG, and CSs@PDA-FA@ICG. (d) (top) Time-dependent profile of the hydrodynamic diameter of CSs@PDA-FA@ICG in PBS or DMEM for 2 weeks; (bottom) optical images of CSs@PDA-FA@ICG with different treatments after 2 weeks.

h. The standard MTT assay was carried out to determine the cell viabilities relative to the untreated control cells. To obtain complementary evidence, biochemical assays of viability were also confirmed via 0.4% Trypan blue staining. For 0.4% trypan blue staining for dead cells, the HeLa cells and normal hepatocytes were incubated with CSs@PDA-FA@ICG (0.10 mg mL^{-1}) for 24 or 48 h. After being washed twice with PBS, the cells were incubated with a trypan blue solution for 15 min followed by cell imaging on a microscope.

2.7. Fluorescence Response of ICG. One milliliter of 0.10 mg mL^{-1} of ICG was mixed with different concentrations of CSs@PDA-FA (0, 0.01, 0.02, 0.05, and 0.10 mg mL^{-1}) for 1 h, and then the fluorescence spectra of all of the samples were recorded with an Edinburgh FLS920 fluorescence spectrophotometer. In vitro time-dependent fluorescence recovery of ICG was measured. HeLa cells (1×10^5 cells/well) were seeded into 96-well plates. After a confluent cellular monolayer covered the inner surface of the plates, CSs@PDA-FA@ICG (0.10 mg mL^{-1}) in DMEM were incubated with or without the attached cells at 37 °C. NIR fluorescence images and fluorescence signal were then detected with a Nikon inverted CMS DM-4000 M fluorescence microscope and Edinburgh FLS920 fluorescence spectrophotometer.

2.8. Targeting Ability of CSs@PDA-FA@ICG NCs. HeLa cells and hepatocytes were respectively seeded in 24-well plates at a density of 1×10^4 cells/well/100 μL. After being incubated for 24 h, the cells were treated with free ICG, CSs@PDA-FA@ICG, and FA+CSs@PDA-FA@ICG at a final equivalent concentration of 0.10 mg mL^{-1}. Under the same conditions, the hepatocytes were treated with CSs@PDA-FA@ICG NCs. After being incubated for 4 h at 37 °C, the cells were washed three times. Subsequently, images of cells were acquired using a Nikon inverted CMS DM-4000 M fluorescence microscope. For the cellular uptake of the NCs to be determined, the HeLa cells were coincubated with CSs@PDA-FA@ICG NCs for 4 h and washed with PBS. A portion of the cells were prepared and imaged under transmission electron microscopy (TEM).

2.9. Measurement of Photothermal Performance. To evaluate the photothermal conversion performance, we irradiated CSs, CSs@PDA-FA, free ICG, and CSs@PDA-FA@ICG at the same concentration by an NIR laser (808 nm) at 1.0 W cm^{-2} for 12 min. Then, the CSs@PDA-FA@ICG NCs with different concentrations were suspended in a quartz cuvette (total volume of 1.0 mL) and irradiated by an NIR laser (808 nm, 1.0 W cm^{-2}).

2.10. Detection of Reactive Oxygen Species (ROS). DCFH-DA was employed to evaluate the ROS generation of CSs@PDA-FA, free ICG, and CSs@PDA-FA@ICG. CSs@PDA-FA, free ICG, and CSs@PDA-FA@ICG were each mixed with DCFH-DA (25 μg mL^{-1}) in water.[33] Then, the mixture solutions were irradiated with an NIR laser (808 nm, 1.0 W cm^{-2}). DCFH-DA fluorescence was excited with a 488 nm wavelength light source.

2.11. Phototherapy. HeLa cells were incubated with 0.10 mg mL^{-1} of CSs@PDA-FA, free ICG, and CSs@PDA-FA@ICG. After 4 h at 37 °C, the cells were washed three times. Next, the cells were irradiated with an NIR laser (808 nm, 1.0 W cm^{-2}) for 6 min. Then, the cells were stained with 0.4% trypan blue and imaged by microscopy. To further quantitatively assess the photothermal and photodynamic cytotoxicity of CSs@PDA-FA@ICG NCs, we incubated HeLa cells with NCs in 96-well plates at 37 °C in a humidified atmosphere containing 5% CO_2 for 4 h. After exposure to the NIR laser (808 nm, 1.0 W cm^{-2}) for 6 min, the cells were left to incubate for another 24 h. Next, MTT assays were carried out to evaluate the cell viability.

DOI: 10.1021/acsami.5b02037
ACS Appl. Mater. Interfaces 2016, 8, 15013−15023

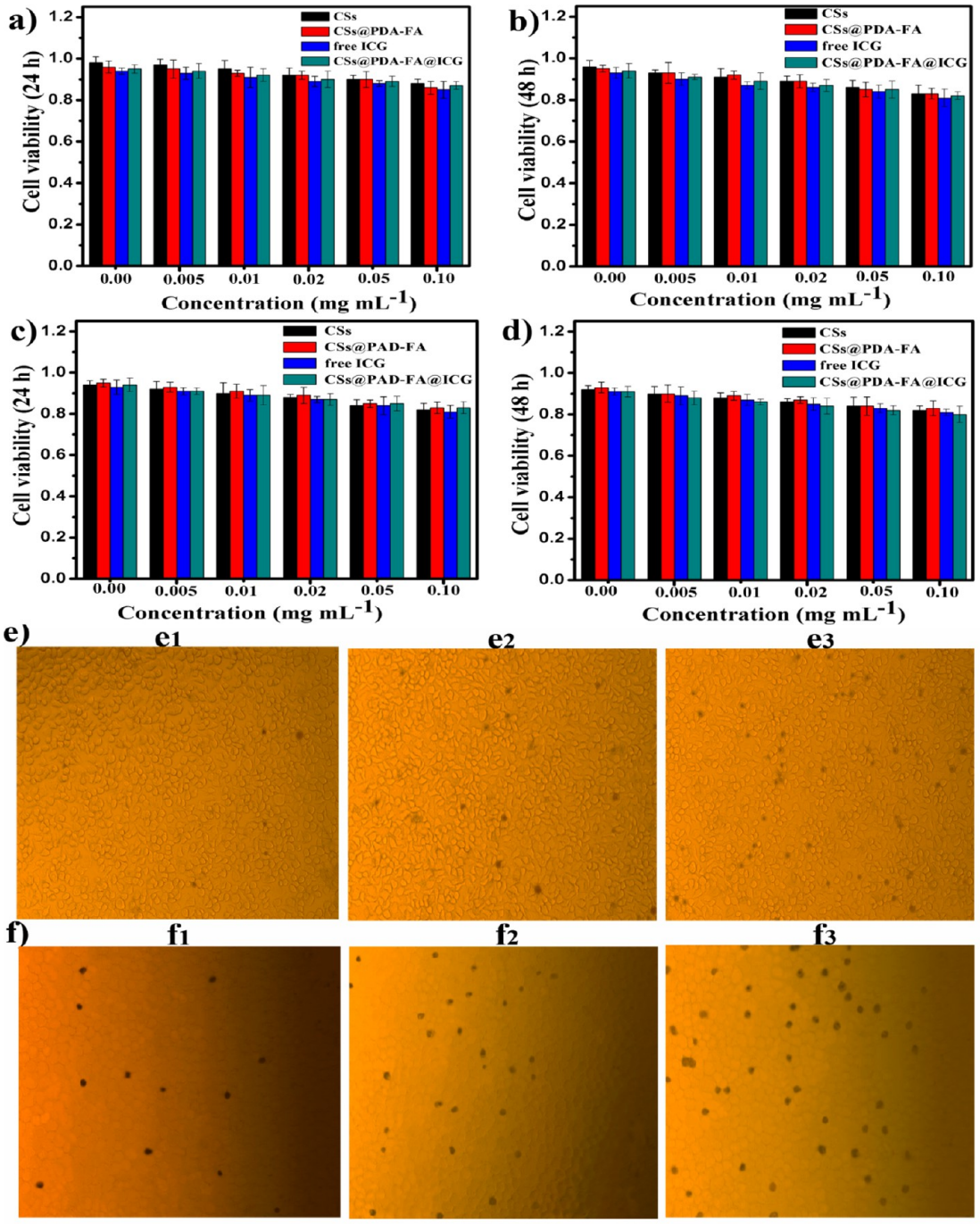

Figure 4. Cell viability of the HeLa cells at different concentrations of nanoparticles for 24 h (a) and 48 h (b) by MTT analysis and the cell viability of hepatocytes at different concentrations of nanoparticles for 24 h (c) and 48 h (d) by MTT analysis. (e, f) Tyrpan blue stained images of HeLa cells (e) and hepatocytes (f): (e_1, f_1) without any treatment, (e_2, f_2) with CSs@PDA-FA@ICG (0.10 mg mL^{-1}) incubation for 24 h, (e_3, f_3) with CSs@PDA-FA@ICG (0.10 mg mL^{-1}) incubation for 48 h.

3. RESULTS AND DISCUSSION

Transmission electron microscopy (TEM) was utilized to investigate the morphology of CSs, CSs@PDA, and CSs@PDA-FA@ICG. As shown in Figure 2a, the TEM images revealed vividly that the rough PDA shell was wrapped onto the smooth surface of the spherical CSs after self-polymerization of the DA in an alkaline solution. TEM images showed that there were no obvious changes in the structure of the CSs@PDA before and after the conjugation and loading with FA and ICG. The hydrodynamic diameter of the modified CS NCs was measured by dynamic light scattering (DLS) analysis with nanoparticles dispersed in phosphate buffered saline (PBS, pH 7.5) by sonication. Figure 2b shows that the hydrodynamic diameter of the CS NPs was gradually increased with the PDA coating, FA conjugation, and ICG loading. The polydispersity index (PDI), reflecting the dispersity of nanoparticles, was less than 0.05, which indicates excellent monodispersity of the nanoparticles. Moreover, the surface modifications on the CSs could be reflected by the change in the zeta potential. Figure 2c shows the zeta potential of functionalized CSs in PBS at pH 7.5. Because of the presence of hydroxyl and carboxyl groups on

DOI: 10.1021/acsami.5b02037
ACS Appl. Mater. Interfaces 2016, 8, 15013−15023

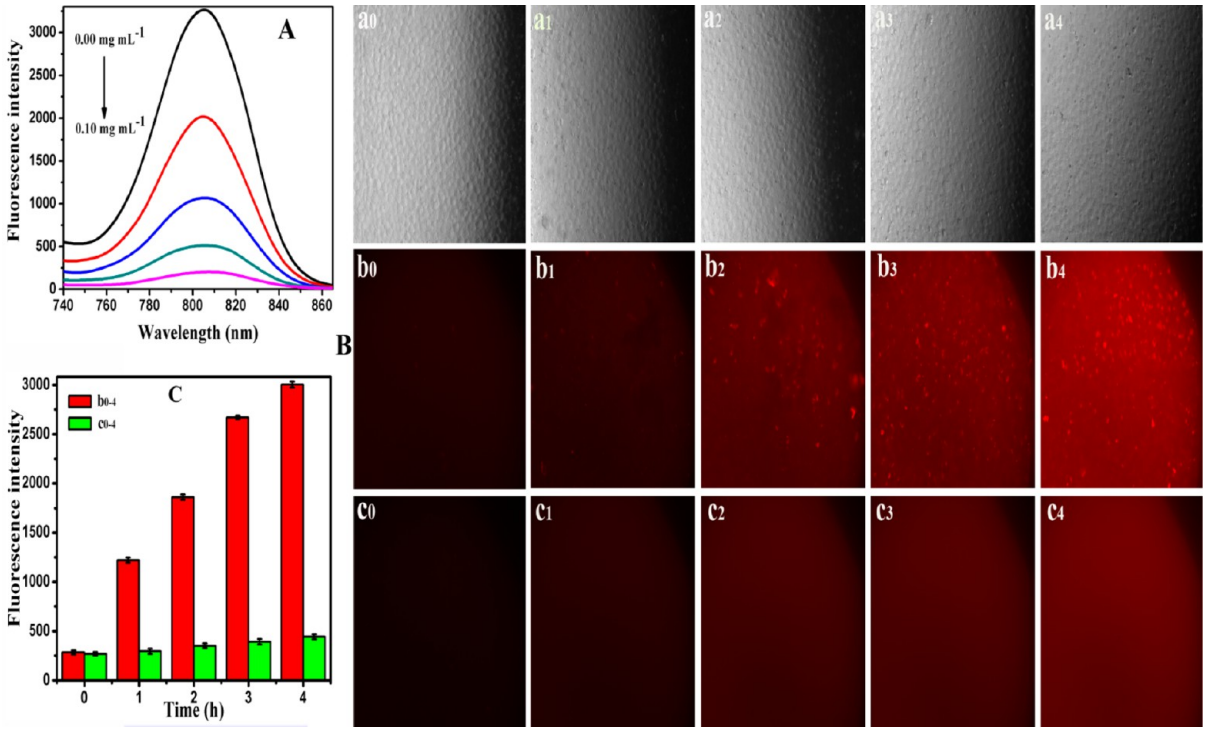

Figure 5. (A) Fluorescence quenching of 0.10 mg mL^{-1} of free ICG in the presence of CSs@PDA-FA over a series of concentrations (0, 0.01, 0.02, 0.05, and 0.10 mg mL^{-1}). (B) NIR images of ICG in culture medium coincubated with HeLa cells (b) or without cells (c); (a_0–a_4) bright field images of HeLa cells; (b_0–b_4) images of HeLa cells coincubated with NCs from 0 to 4 h in dark field; (c_0–c_4) images of culture medium coincubated with NCs from 0 to 4 h in dark field. (C) NIR fluorescence intensity change of ICG in culture medium coincubated with HeLa cells (b) or without cells (c) from 0 to 4 h.

CSs, the zeta potential of CSs was −30.5 ± 2.6 mV. After the PDA coating, the zeta potential of CSs@PDA became −13.7 ± 3.2 mV due to the existence of amino and hydroxyl groups. Although some amino-groups accreted on the surface of PDA, there were a significant number of hydroxyl groups on the surface of PDA. Under alkaline conditions, the zeta potential of PDA would be negative. However, upon successful conjugation with FA, the zeta potential of CSs@PDA-FA was decreased to −20.6 ± 2.2 mV because of the existence of a large number of COOH groups of FA. After the ICG loading, the zeta potential of CSs@PDA-FA@ICG was −38.5 ± 1.9 mV because of the existence of SO_3 groups on the surface of ICG. In conclusion, the changes in the diameters and zeta potentials of these nanoparticles after being coated, conjugated, and loaded confirmed the successful construction of CSs@PDA-FA@ICG NCs.

The optical property of the CSs@PDA-FA@ICG NC aqueous dispersion was subsequently studied by UV–vis absorbance and fluorescence emission spectra. Figure 3a shows the photographs of different nanoparticles in PBS. Different from as-prepared CSs, which were a brown-red color in PBS, CSs@PDA were a darker brown color. However, after the FA modification, CSs@PDA-FA appeared as a brown-yellow color. Ultimately, the CSs@PDA-FA@ICG NCs appeared as a black-green color, indicating successful loading of ICG. After centrifugation, the precipitate and change of solution color were observed for CSs, CSs@PDA, CSs@PDA-FA, and CSs@PDA-FA@ICG, showing the existence of small FA and ICG in solution. We detected the UV–vis absorbance spectra of different nanoparticle solutions with the same concentration (0.05 mg mL^{-1}) in PBS. Figure 3b showed the CSs and CSs@PDA with no absorption in the range of 300–800 nm. CSs@PDA-FA displayed the characteristic FA peak at ∼295 nm, indicating the successful conjugation of FA onto the CSs@PDA. The maximum NIR absorption peak of CSs@PDA-FA@ICG was not only consistent with the dominant monomeric absorption peak of free ICG dissolved in PBS but also induced an extra absorption peak at ∼295 nm. Subsequently, the shapes of the NIR fluorescence emission spectra for CSs@PDA-FA@ICG were similar to that of free ICG, whereas there was no fluorescence emission peak for CSs@PDA-FA (Figure 3c). Herein, the ICG loading efficiency was evaluated up to 58.9% according to UV–vis absorbance (Table S1, Supporting Information), which would enhance delivery of ICG into cancer cells for bioapplications. These results suggest successful loading of ICG and no degradation of ICG during the functionalization process. Therefore, the optical properties of CSs@PDA-FA@ICG with NIR absorbance and emission can be exploited to establish the nanocarriers for NIR imaging in biological systems.

After confirming the successful construction of CSs@PDA-FA@ICG NCs, we then evaluated NCs' stability and toxicity for bioapplications. The prepared CSs, ICG, and CSs@PDA-FA@ICG exhibited excellent dispersivity and stability in a range of solutions, including water, PBS, cell medium, and fetal serum (Figure S1, Supporting Information). Furthermore, DLS was used to determine the colloidal stability of CSs@PDA-FA@ICG dispersed in PBS or DMEM. The time-dependent profile of the effective diameter of the CSs@PDA-FA@ICG is shown in Figure 3d. The diameter of CSs@PDA-FA@ICG after 2 weeks remained the same size without evident variation, exhibiting good colloidal stability in PBS or DMEM. In addition, as seen in the optical images, the CSs@PDA-FA@

DOI: 10.1021/acsami.5b02037
ACS Appl. Mater. Interfaces 2016, 8, 15013–15023

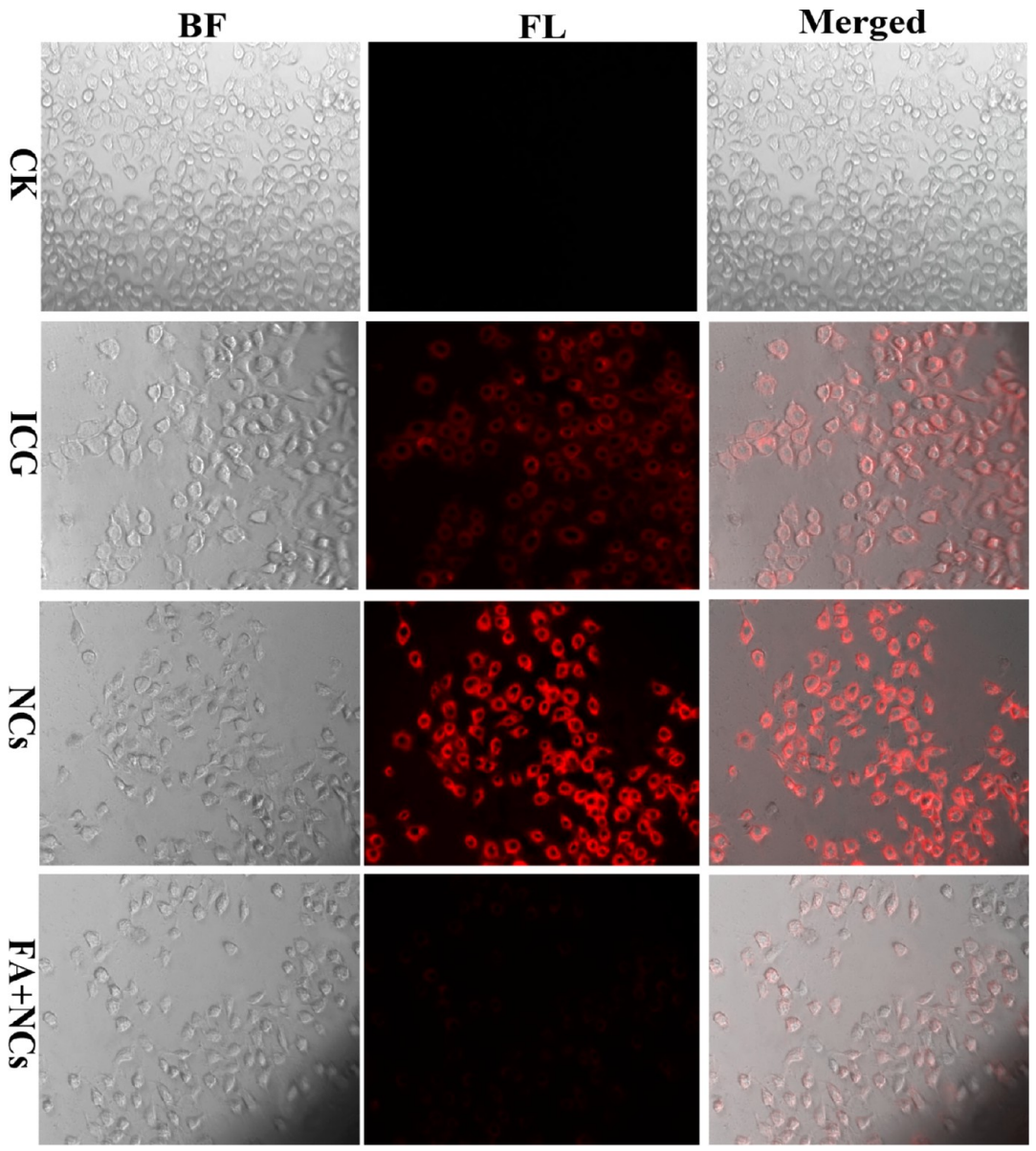

Figure 6. Microscopy images of HeLa cells after treatment with ICG, CSs@PDA-FA@ICG, or FA+CSs@PDA-FA@ICG for 4 h. The CK group had no treatment; BF, bright field; FL, fluorescence imaging.

ICG still retained good monodispersity in PBS and DMEM for over 2 weeks, which showed no obvious precipitation.

For further biomedicine applications, the intrinsic toxicity of CSs, CSs@PDA-FA, ICG, and CSs@PDA-FA@ICG was studied by MTT assay. HeLa cells and normal hepatocytes were respectively incubated with various concentrations of nanoparticles for 24 and 48 h (Figure 4a–d). We found that the treated cells remained over 80% viable even at the highest concentration. We also investigated the behavior of CSs@PDA-FA@ICG in living cells (HeLa cells and normal hepatocytes) through observations of the morphological changes and color changes of cells using a microscope (Figure 4e, f). For 0.4% trypan blue staining for dead cells (green color, due to superposition of yellow and blue color), the microscope images illustrated no obvious difference in the cancer and normal cell morphology and the rarely stained cells. These results indicated the low biological toxicity of CSs and their nanocomposites over a wide concentration range. As is known, many carbon nanomaterials with different shapes (for example, carbon nanotubes and graphene) have previously been proposed for various biomedical applications.[34−36] These carbon nanomaterials exhibit relatively low toxicity. Nevertheless, it has been reported that the cell viability of graphene and carbon nanotubes was below 50% at the concentration of 0.10 mg mL^{-1} for 24 h.[37] Furthermore, it had been reported that the cell viability of CSs was retained at more than 80% at a concentration of 0.10 mg mL^{-1} for 24 h, which is consistent with our results.[38] Thus, CSs can serve as a safe carrier. Moreover, the harmless PDA biofilms can reduce the toxicity of biomaterials, and ICG as a safe clinical drug has been widely applied for biomedicine.[39−42] Therefore, the fabricated CSs@PDA-FA@ICG NCs with good biocompatibility and low toxicity could serve as a safe drug carrier and contrast agent for bioapplications.

To elucidate the mechanism of NIR fluorescent turn off/on of the nanoprobes, we investigated the capability of the CSs@PDA-FA@ICG as a nanoprobe for adsorption and fluorescence quenching in vitro and the cellular fluorescence recovery of

DOI: 10.1021/acsami.5b02037
ACS Appl. Mater. Interfaces 2016, 8, 15013−15023

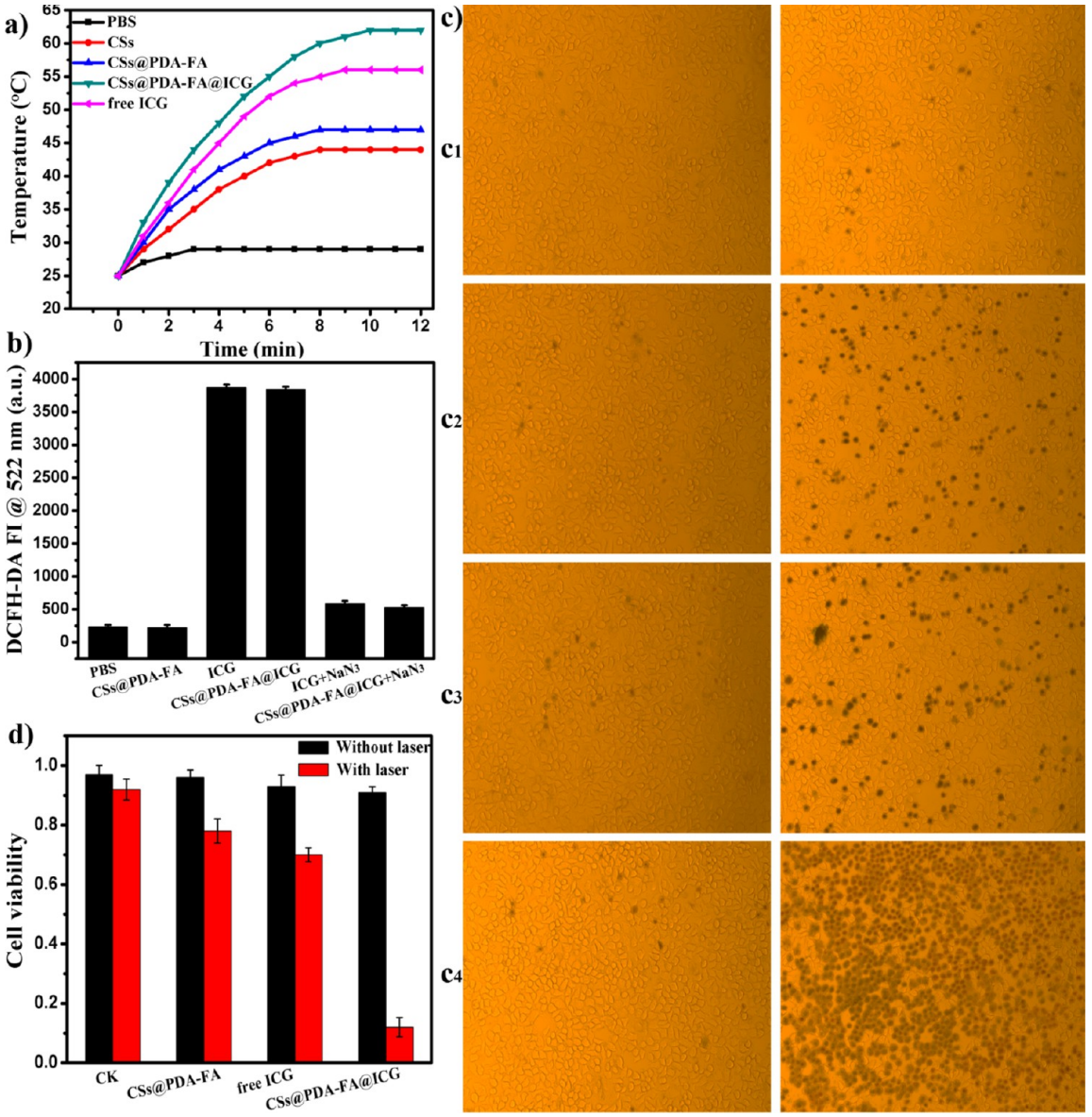

Figure 7. (a) Temperature changes of PBS, CSs, CSs@PDA-FA, CSs@PDA-FA@ICG, and ICG solutions in response to irradiation by an NIR laser (808 nm) with a power density of 1.0 W cm^{-2}. (b) DCFH-DA fluorescence intensity at 522 nm in PBS, CSs@PDA-FA, ICG, CSs@PDA-FA@ICG, ICG (±10 μM NaN_3), and CSs@PDA-FA@ICG (±10 μM NaN_3) solutions after 808 nm laser irradiation. (c) Phototoxicity of CSs@PDA-FA (c_2), ICG (c_3), and CSs@PDA-FA@ICG (c_4) on HeLa cells with 808 nm laser irradiation for 6 min. (c_1) Phototoxicity of HeLa cells with 808 nm laser irradiation alone for 6 min. Dead cells were stained with tyrpan blue. (d) Quantitative detection of HeLa cell viability by MTT assay. CK groups without and with irradiation by the 808 nm laser. The cells were treated with CSs@PDA-FA, ICG, and CSs@PDA-FA@ICG.

ICG. First, the adsorption and fluorescence quenching abilities of the CSs@PDA-FA toward ICG were evaluated by mixing the fluorescent ICG and the prepared CSs@PDA-FA. As shown in Figure 5A, the fluorescence of the ICG was almost entirely quenched in the presence of 0.10 mg mL^{-1} of CSs@PDA-FA, indicating strong adsorption of the ICG onto the CSs@PDA-FA and high fluorescence quenching efficiency of the CSs@PDA-FA. The high fluorescence quenching efficiency made CSs@PDA-FA function as the fluorescence's off switch. After assessing the in vitro response of the CSs@PDA-FA to ICG, we then validated whether the quenched fluorescence of CSs@PDA-FA@ICG could recover in an intracellular environment. A large number of HeLa cells were incubated with CSs@PDA-FA@ICG in cell culture. As shown in Figure 5B, the NIR fluorescence images were obtained as a function of time. The b row contains HeLa cells in culture medium, whereas the c row contains only culture medium. The background of both rows are red due to a small amount of fetal calf serum (including some protein) in the culture medium. Upon being incubated for prolonging amounts of time, the little amount of ICG in NCs could bind with the protein in the cell medium and recover fluorescence. The fluorescence in the cell group became much stronger over time, whereas the fluorescence in the medium over time in the absence of HeLa cells had only a slight change. The results indicated that, after CSs@PDA-FA@ICG entered cells, proteins (e.g., glutathione S-transferase) in the intracellular microenvironment had very strong adsorption to ICG, leading to the recovery of ICG fluorescence. The NIR fluorescence intensity was also evaluated via a fluorescence spectrometer, and an approximate 10× increase in fluorescence

DOI: 10.1021/acsami.5b02037
ACS Appl. Mater. Interfaces 2016, 8, 15013−15023

intensity was observed in CSs@PDA-FA@ICG-treated HeLa cells after 4 h compared with that of the control (Figure 5C). These resuts showed that the NIR fluorescence of CSs@PDA-FA@ICG NCs could be effectively activated (high signal) in the intracellular environment, whereas a low signal was detected (low noise) in a nonstimulating environment. The S/N ratio can be improved through the design of the nanoparticles, the signal of which can be amplified in specific environments, but otherwise remains undetectable. A high S/N ratio is significant for enhancing the sensitivity and resolution of imaging.[43−45] All of the results described above demonstrate that CSs@PDA-FA@ICG was a sensitive "OFF" to "ON" nanoprobe that can be effectively used for cancer imaging due to activated NIR fluorescence in an intracellular environment.

After examining the signaling ability of the CSs@PDA-FA@ICG nanoprobe, we further validated the capability of CSs@PDA-FA@ICG in targeted imaging of HeLa cancers in which the FA receptor is overexpressed. The NIR fluorescence images demonstrated that HeLa cells treated with free ICG displayed a red fluorescence via passive uptake compared with that of the control group (Figure 6). However, the red fluorescence of the HeLa cells incubated with the CSs@PDA-FA@ICG nanoprobe under the same conditions became much stronger than those treated with ICG, indicating the specific binding of CSs@PDA-FA@ICG to the FA receptors overexpressed on the HeLa cells. Strong fluorescence in the CSs@PDA-FA@ICG-treated HeLa cells was observed by a fluorescence microscope due to FA active-targeting mediated endocytosis of the nanoprobe and dequenching of ICG fluorescence with 4 h of incubation. We also performed competitive binding assay experiments in which HeLa cells were first incubated at 37 °C with free FA for 2 h and then incubated with CSs@PDA-FA@ICG for another 4 h. The NIR fluorescence signal became very weak upon adding the free FA. Moreover, the ability of NCs to interact with FA-negative normal hepatocytes was also assessed. Figure S2 in the Supporting Information showed little uptake of the NCs with relatively weak fluorescence signals, which further confirmed the highly specific targeting capability of the as-prepared CSs@PDA-FA@ICG NCs to FA-positive HeLa cancer cells. Furthermore, the CSs@PDA-FA@ICG bound to the FA receptor was then internalized by HeLa cells. In Figure S3 in the Supporting Information, it was clearly observed that many CSs@PDA-FA@ICG NCs were confined to the cytoplasm. These results demonstrate that the CSs@PDA-FA@ICG-based nanoprobe can be used to detect cancer cells by targeted NIR imaging.

Notably, CSs@PDA-FA@ICG served not only as an NIR imaging agent but also as an NIR light absorber in photothermal and photodynamic cancer therapy. Phototherapy with high selectivity as well as minimum side effects for normal tissues has caused significant attention for cancer treatment. To investigate the photothermal efficiency of CSs@PDA-FA@ICG NCs, we dispersed the CNs in PBS at concentrations ranging from 0.005 to 0.10 mg mL^{-1} and irradiated them with an 808 nm laser at a power density of 1.0 W cm^{-2} for 12 min. As shown in Figure S4 in the Supporting Information, the temperature of the CSs@PDA-FA@ICG solutions increased more rapidly with the material concentration and the radiant time. At concentrations of 0.10 mg mL^{-1}, the temperature elevation was >60 °C. Herein, the photothermal efficiency of PBS, CSs, CSs@PDA-FA, free ICG, and CSs@PDA-FA@ICG (with the same concentration) was evaluated and compared (Figure 7a). Upon NIR laser irradiation, the temperature of CSs, CSs@PDA-FA, free ICG, and CSs@PDA-FA@ICG increased to 44, 48, 57, and 62 °C, respectively, whereas the PBS alone only increased to 29 °C. The results showed that NCs had a synergistic impact on improving light-thermal conversion efficiency. Moreover, the photothermal efficiency of CSs@PDA-FA@ICG NCs was even slightly enhanced compared with that of free ICG, indicating that the fluorescence quenching of ICG did not affect the light-thermal conversion of NCs. The measurement proved that CSs@PDA-FA@ICG NCs had a higher photothermal efficiency than that of free ICG or CSs. The results described above demonstrated that the CSs@PDA-FA@ICG NCs that integrated the photoconversion performance of CSs, PDA, and ICG into a single system could be applied as effective photothermal agents.

Furthermore, the process of the photothermal response of CSs@PDA-FA@ICG NCs was accompanied by the generation of ROS, which could be used for PDT. Thus, the photodynamic efficiency of NCs was measured according to the fluorescence signal of DCFH-DA at 522 nm. As shown in Figure S5 in the Supporting Information, the fluorescence intensity of DCFH-DA generation from free ICG and CSs@PDA-FA@ICG NCs increased upon prolonged laser irradiation time, indicating continuous generation of ROS upon NIR laser irradiation. However, the fluorescence intensities remained unaltered upon laser irradiation for the systems with DCFH-DA alone or a mixture of DCFH-DA and CSs@PDA-FA. When sodium azide (NaN_3, a well-known ROS scavenger) was added, the fluorescence signal of DCFH-DA in ICG or CSs@PDA-FA@ICG NCs solutions was obviously inhibited, further proving the generation of ROS during laser irradiation (Figure 7b). Thus, these results demonstrate that the CSs@PDA-FA@ICG could adequately convert the NIR laser energy to ROS and heat, making it a useful photothermal and photodynamic agent.

Inspired by these results, we further evaluated the PTT/PDT efficiency of CSs@PDA-FA@ICG NCs. The HeLa cells were incubated with 0.10 mg mL^{-1} of CSs@PDA-FA, ICG, and CSs@PDA-FA@ICG for 4 h and were then irradiated by an 808 nm laser at a power density of 1.0 W cm^{-2} for 6 min. After this treatment, HeLa cells were stained with 0.4% trypan blue, which only incorporates into dead cells. In trypan blue staining for the dead cell experiment, we observed that the CSs@PDA-FA and ICG could only kill a portion of the cancer cells, whereas CSs@PDA-FA@ICG killed almost all of the cancer cells (Figure 7c). These phenomena showed that CSs@PDA-FA served as the ICG carrier for improving the stability and specificity of ICG to enhance the treatment efficiency. Moreover, the targeted CSs@PDA-FA@ICG NCs can integrate the photoconversion performance of CSs, PDA, and ICG into one system for efficient phototherapy. Thus, CSs@PDA-FA@ICG NCs can kill more cancer cells than CSs@PDA-FA or ICG alone. In addition, the images also illustrated that laser irradiation alone was quite safe for HeLa cells. The results suggested that the phototherapy triggered by single 808 nm irradiation of CSs@PDA-FA@ICG significantly boosted the cytotoxic effect of the targeted NCs on cancer cells.

Next, the PTT/PDT efficiency of CSs@PDA-FA@ICG was also evaluated by MTT assays (Figure 7d). At first, no obvious cytotoxicity was observed when HeLa cells were treated only with NIR laser irradiation. However, when CSs@PDA-FA was used, the viability of cells was maintained well without NIR laser irradiation but decreased to 76% with NIR laser irradiation. Similarly, when ICG was used, the viability of cells was also maintained well without NIR laser irradiation but

DOI: 10.1021/acsami.5b02037
ACS Appl. Mater. Interfaces 2016, 8, 15013−15023

decreased to 70% with NIR laser irradiation. Nevertheless, there was a very obvious difference among CSs@PDA-FA@ICG, CSs@PDA-FA, and free ICG. The CSs@PDA-FA@ICG with laser group induced the death of up to 91% of cells, suggesting that CSs@PDA-FA@ICG could effectively target FA overexpressing HeLa cells and improve PTT/PDT therapy by a single NIR laser. The MTT assay was consistent with the staining images of live/dead cells. Therefore, the simultaneous synergistic PTT/PDT induced by the biocompatible CSs@PDA-FA@ICG NCs with a single NIR laser could enhance phototherapy efficiency of cancer cells. In sum, our preliminary experiment demonstrates the feasibility of using CSs@PDA-FA@ICG NCs as an ideal NIR fluorescent turn-on nanoprobe for cancer cell detection and as PTT/PDT agents for effective cancer cell treatment.

4. CONCLUSIONS

In summary, we have successfully fabricated facile and green CSs@PDA-FA@ICG NCs through the self-assembly of a core CS-coated PDA with ICG for activatable NIR imaging and effective phototherapy of cancer cells. The prepared CSs@PDA-FA@ICG NCs display a targeted, sensitive switch-control property: activated fluorescence from "OFF" to "ON" and high specificity achieved by FA receptor-mediated targeting. These features render the NCs very attractive due to their ability to implement sensitive imaging and detection of cancer cells. In vitro assays reveal that CSs@PDA-FA provides a sensitive and selective quencher for NIR fluorescence of ICG. Live cell studies show that the NIR fluorescence of ICG can be recovered in an intracellular environment and that CSs@PDA-FA@ICG can be used as a highly sensitive contrast agent. Moreover, because of the strong NIR absorption of the CSs, PDA, and ICG, the CSs@PDA-FA@ICG NCs can be employed for simultaneously synergetic PTT/PDT with a single NIR laser irradiation. Additionally, the CSs@PDA-FA@ICG NCs exhibited excellent size stability and water dispersibility, low cytotoxicity, good biocompatibility, high ICG loading capacity, high specificity, and strong near-infrared absorbance. In light of these advantages, CSs@PDA-FA@ICG NCs have the potential to be a targeted NIR fluorescent turn-on nanoprobe for activation-inducable imaging and effective phototherapy of cancer cells. Thus, we anticipate that more PDA-coated carbon nanomaterials will be developed and used to design novel multifunctional nanocomposites for cancer imaging and phototherapy.

■ ASSOCIATED CONTENT

Supporting Information

The ICG loading efficiency, the stability of nanoparticles in various solutions, microscopy images of normal hepatocytes, TEM images of HeLa cell sections, the temperature change of CSs@PDA-FA@ICG NCs at various concentrations under irradiation, and the photodynamic efficiency of ICG and CSs@PDA-FA@ICG NCs. The Supporting Information is available free of charge on the ACS Publications website at DOI: 10.1021/acsami.5b02037.

■ AUTHOR INFORMATION

Corresponding Author

*E-mail: hyhan@mail.hzau.edu.cn. Fax: +86-27-87288505. Tel: +86-27-87288505.

Notes

The authors declare no competing financial interest.

■ ACKNOWLEDGMENTS

This work was financially supported by the Fundamental Research Funds for the Central Universities (2012SC04) and the National Natural Science Foundation of China (21175051, 21375043).

■ REFERENCES

(1) Lee, D.-E.; Koo, H.; Sun, I.-C.; Ryu, J. H.; Kim, K.; Kwon, I. C. Multifunctional Nanoparticles for Multimodal Imaging and Theragnosis. *Chem. Soc. Rev.* **2012**, *41*, 2656−2672.

(2) Skeete, Z.; Cheng, H.; Crew, E.; Lin, L.; Zhao, W.; Joseph, P.; Shan, S.; Cronk, H.; Luo, J.; Li, Y.; Zhang, Q.; Zhong, C.-J. Design of Functional Nanoparticles and Assemblies for Theranostic Applications. *ACS Appl. Mater. Interfaces* **2014**, *6*, 21752−21768.

(3) Chen, Z.; Li, Z.; Wang, J.; Ju, E.; Zhou, L.; Ren, J.; Qu, X. A Multi-Synergistic Platform for Sequential Irradiation-Activated High-Performance Apoptotic Cancer Therapy. *Adv. Funct. Mater.* **2014**, *24*, 522−529.

(4) Monaco, A. M.; Giugliano, M. Carbon-Based Smart Nanomaterials in Biomedicine and Neuroengineering. *Beilstein J. Nanotechnol.* **2014**, *5*, 1849−1863.

(5) Gong, H.; Peng, R.; Liu, Z. Carbon Nanotubes for Biomedical Imaging: The Recent Advances. *Adv. Drug Delivery Rev.* **2013**, *65*, 1951−1963.

(6) Kim, T.-W.; Chung, P.-W.; Slowing, I. I.; Tsunoda, M.; Yeung, E. S.; Lin, V. S.-Y. Structurally Ordered Mesoporous Carbon Nanoparticles as Transmembrane Delivery Vehicle in Human Cancer Cells. *Nano Lett.* **2008**, *8*, 3724−3727.

(7) Li, M.; Li, W.; Liu, S. Hydrothermal Synthesis, Characterization, and KOH Activation of Carbon Spheres from Glucose. *Carbohyd. Res.* **2011**, *346*, 999−1004.

(8) Fang, Y.; Gu, D.; Zou, Y.; Wu, Z.; Li, F.; Che, R.; Deng, Y.; Tu, B.; Zhao, D. A Low-Concentration Hydrothermal Synthesis of Biocompatible Ordered Mesoporous Carbon Nanospheres with Tunable and Uniform Size. *Angew. Chem., Int. Ed.* **2010**, *49*, 7987−7991.

(9) Liu, X.; Jiang, H.; Ge, W.; Wu, C.; Chen, D.; Li, Q.; Chen, Y.; Wang, X. Green and Facile Synthesis of Highly Biocompatible Carbon Nanospheres and Their pH-Responsive Delivery of Doxorubicin to Cancer Cells. *RSC Adv.* **2015**, *5*, 17532−17540.

(10) Xu, G.; Liu, S.; Niu, H.; Lv, W.; Wu, R. Functionalized Mesoporous Carbon Nanoparticles for Targeted Chemo-Photothermal Therapy of Cancer Cells under Near-Infrared Irradiation. *RSC Adv.* **2014**, *4*, 33986−33997.

(11) Zhou, L.; Dong, K.; Chen, Z.; Ren, J.; Qu, X. Near-Infrared Absorbing Mesoporous Carbon Nanoparticle as an Intelligent Drug Carrier for Dual-Triggered Synergistic Cancer Therapy. *Carbon* **2015**, *82*, 479−488.

(12) Wan, L.; Zhao, Q.; Zhao, P.; He, B.; Jiang, T.; Zhang, Q.; Wang, S. Versatile Hybrid Polyethyleneimine-Mesoporous Carbon Nanoparticles for Targeted Delivery. *Carbon* **2014**, *79*, 123−134.

(13) Lin, L.; Cong, Z.; Cao, J.; Ke, K.; Peng, Q.; Gao, J.; Yang, H.; Liu, G.; Chen, X. Multifunctional Fe_3O_4@Polydopamine Core-Shell Nanocomposites for Intracellular mRNA Detection and Imaging-Guided Photothermal Therapy. *ACS Nano* **2014**, *8*, 3876−3883.

(14) Black, K. C.; Yi, J.; Rivera, J. G.; Zelasko-Leon, D. C.; Messersmith, P. B. Polydopamine-Enabled Surface Functionalization of Gold Nanorods for Cancer Cell-Targeted Imaging and Photothermal Therapy. *Nanomedicine* **2013**, *8*, 17−28.

(15) Liu, X.; Cao, J.; Li, H.; Li, J.; Jin, Q.; Ren, K.; Ji, J. Mussel-Inspired Polydopamine: A Biocompatible and Ultrastable Coating for Nanoparticles *In Vivo*. *ACS Nano* **2013**, *7*, 9384−9395.

(16) Lee, H.; Rho, J.; Messersmith, P. B. Facile Conjugation of Biomolecules onto Surfaces via Mussel Adhesive Protein Inspired Coatings. *Adv. Mater.* **2009**, *21*, 431−434.

(17) Liu, Y.; Ai, K.; Liu, J.; Deng, M.; He, Y.; Lu, L. Dopamine-Melanin Colloidal Nanospheres: An Efficient Near-Infrared Photothermal Therapeutic Agent for *In Vivo* Cancer Therapy. *Adv. Mater.* **2013**, *25*, 1353−1359.
(18) Yang, S. J.; Lin, F. H.; Tsai, K. C.; Wei, M. F.; Tsai, H. M.; Wong, J. M.; Shieh, M. J. Folic Acid-Conjugated Chitosan Nanoparticles Enhanced Protoporphyrin IX Accumulation in Colorectal Cancer Cells. *Bioconjugate Chem.* **2010**, *21*, 679−689.
(19) Chen, N.; Shao, C.; Qu, Y.; Li, S.; Gu, W.; Zheng, T.; Ye, L.; Yu, C. Folic Acid-Conjugated MnO Nanoparticles as a T1 Contrast Agent for Magnetic Resonance Imaging of Tiny Brain Gliomas. *ACS Appl. Mater. Interfaces* **2014**, *6*, 19850−19857.
(20) Sheng, Z.; Hu, D.; Zheng, M.; Zhao, P.; Liu, H.; Gao, D.; Gong, P.; Gao, G.; Zhang, P.; Ma, Y.; Cai, L. Smart Human Serum Albumin-Indocyanine Green Nanoparticles Generated by Programmed Assembly for Dual-Modal Imaging-Guided Cancer Synergistic Phototherapy. *ACS Nano* **2014**, *8*, 12310−12322.
(21) Mizrahi, D. M.; Ziv-Polat, O.; Perlstein, B.; Gluz, E.; Margel, S. Synthesis, Fluorescence and Biodistribution of a Bone-Targeted Near-Infrared Conjugate. *Eur. J. Med. Chem.* **2011**, *46*, 5175−5183.
(22) Ma, Y.; Sadoqi, M.; Shao, J. Biodistribution of Indocyanine Green-Loaded Nanoparticles with Surface Modifications of PEG and Folic Acid. *Int. J. Pharm.* **2012**, *436*, 25−31.
(23) Zheng, X.; Zhou, F.; Wu, B.; Chen, W. R.; Xing, D. Enhanced Tumor Treatment Using Biofunctional Indocyanine Green-Containing Nanostructure by Intratumoral or Intravenous Injection. *Mol. Pharmaceutics* **2012**, *9*, 514−522.
(24) Yu, J.; Javier, D.; Yaseen, M. A.; Nitin, N.; Richards-Kortum, R.; Anvari, B.; Wong, M. S. Self-Assembly Synthesis, Tumour Cell Targeting, and Photothermal Capabilities of Antibody-Coated Indocyanine Green Nanocapsules. *J. Am. Chem. Soc.* **2010**, *132*, 1929−1938.
(25) Altinoglu, E. I.; Russin, T. J.; Kaiser, J. M.; Barth, B. M.; Eklund, P. C.; Kester, M.; Adair, J. H. Near-Infrared Emitting Fluorophore-Doped Calcium Phosphate Nanoparticles for *In Vivo* Imaging of Human Breast Cancer. *ACS Nano* **2008**, *2*, 2075−2084.
(26) Hannah, A.; Luke, G.; Wilson, K.; Homan, K.; Emelianov, S. Indocyanine Green-Loaded Photoacoustic Nanodroplets: Dual Contrast Nanoconstructs for Enhanced Photoacoustic and Ultrasound Imaging. *ACS Nano* **2014**, *8*, 250−259.
(27) Wang, Y.; Huang, R.; Liang, G.; Zhang, Z.; Zhang, P.; Yu, S.; Kong, J. MRI-Visualized, Dual-Targeting, Combined Tumor Therapy Using Magnetic Graphene-Based Mesoporous Silica. *Small* **2014**, *10*, 109−116.
(28) Wen, H.; Dong, C.; Dong, H.; Shen, A.; Xia, W.; Cai, X.; Song, Y.; Li, X.; Li, Y.; Shi, D. Engineered Redox-Responsive PEG Detachment Mechanism in PEGylated Nano-Graphene Oxide for Intracellular Drug Delivery. *Small* **2012**, *8*, 760−769.
(29) Huang, P.; Xu, C.; Lin, J.; Wang, C.; Wang, X.; Zhang, C.; Zhou, X.; Guo, S.; Cui, D. Folic Acid-Conjugated Graphene Oxide Loaded with Photosensitizers for Targeting Photodynamic Therapy. *Theranostics* **2011**, *1*, 240−250.
(30) Zheng, M.; Yue, C.; Ma, Y.; Gong, P.; Zhao, P.; Zheng, C.; Sheng, Z.; Zhang, P.; Wang, Z.; Cai, L. Single-Step Assembly of DOX/ICG Loaded Lipid-Polymer Nanoparticles for Highly Effective Chemo-Photothermal Combination Therapy. *ACS Nano* **2013**, *7*, 2056−2067.
(31) Kirchherr, A. K.; Briel, A.; Mäder, K. Stabilization of Indocyanine Green by Encapsulation within Micellar Systems. *Mol. Pharmaceutics* **2009**, *6*, 480−491.
(32) Jia, X.; Cai, X.; Chen, Y.; Wang, S.; Xu, H.; Zhang, K.; Ma, M.; Wu, H.; Shi, J.; Chen, H. Perfluoropentane-Encapsulated Hollow Mesoporous Prussian Blue Nanocubes for Activated Ultrasound Imaging and Photothermal Therapy of Cancer. *ACS Appl. Mater. Interfaces* **2015**, *7*, 4579−4588.
(33) Yin, L. Y.; Huang, J. Q.; Huang, W. M.; Li, D. H.; Wang, G. H.; Liu, Y. D. Microcystin-RR-induced Accumulation of Reactive Oxygen Species and Alteration of Antioxidant Systems in Tobacco BY-2 Cells. *Toxicon* **2005**, *46*, 507−512.
(34) Mahmood, M.; Villagarcia, H.; Dervishi, E.; Mustafa, T.; Alimohammadi, M.; Casciano, D.; Khodakovskaya, M.; Biris, A. S. Role of Carbonaceous Nanomaterials in Stimulating Osteogenesis in Mammalian Bone Cells. *J. Mater. Chem. B* **2013**, *1*, 3220−3230.
(35) Kakran, M.; Sahoo, N. G.; Bao, H.; Pan, Y.; Li, L. Carbon Nanomaterials for Drug Delivery. *Curr. Med. Chem.* **2011**, *18*, 4503−4512.
(36) Zhang, Y.; Ali, S. F.; Dervishi, E.; Xu, Y.; Li, Z.; Casciano, D.; Biris, A. S. Cytotoxicity Effects of Graphene and Single-Wall Carbon Nanotubes in Neural Phaeochromocytoma-Derived PC12 Cells. *ACS Nano* **2010**, *4*, 3181−3186.
(37) Hu, W.; Peng, C.; Lv, M.; Li, X.; Zhang, Y.; Chen, N.; Fan, C.; Huang, Q. Protein Corona-Mediated Mitigation of Cytotoxicity of Graphene Oxide. *ACS Nano* **2011**, *5*, 3693−3700.
(38) Zhao, P.; Wang, L.; Sun, C.; Jiang, T.; Zhang, J.; Zhang, Q.; Sun, J.; Deng, Y.; Wang, S. Uniform Mesoporous Carbon as a Carrier for Poorly Water Soluble Drug and Its Cytotoxicity Study. *Eur. J. Pharm. Biopharm.* **2012**, *80*, 535−543.
(39) Hong, S.; Kim, K. Y.; Wook, H. J.; Park, S. Y.; Lee, K. D.; Lee, D. Y.; Lee, H. Attenuation of the *In Vivo* Toxicity of Biomaterials by Polydopamine Surface Modification. *Nanomedicine* **2011**, *6*, 793−801.
(40) Liu, X.; Cao, J.; Li, H.; Li, J.; Jin, Q.; Ren, K.; Ji, J. Mussel-Inspired Polydopamine: A Biocompatible and Ultrastable Coating for Nanoparticles *In Vivo*. *ACS Nano* **2013**, *7*, 9384−9395.
(41) Sheng, Z.; Hu, D.; Xue, M.; He, M.; Gong, P.; Cai, L. Indocyanine Green Nanoparticles for Theranostic Applications. *Nano-Micro Lett.* **2013**, *5*, 145−150.
(42) Saxena, V.; Sadoqi, M.; Shao, J. Polymeric Nanoparticulate Delivery System for Indocyanine Green: Biodistribution in Healthy Mice. *Int. J. Pharm.* **2006**, *308*, 200−204.
(43) Lee, S.; Park, K.; Kim, K.; Choi, K.; Kwon, I. C. Activatable Imaging Probes with Amplified Fluorescent Signals. *Chem. Commun. (Cambridge, U.K.)* **2008**, *36*, 4250−4260.
(44) Lee, S.; Ryu, J. H.; Park, K.; Lee, A.; Lee, S.-Y.; Youn, I.-C.; Ahn, C.-H.; Yoon, S. M.; Myung, S.-J.; Moon, D. H.; Chen, X.; Choi, K.; Kwon, I. C.; Kim, K. Polymeric Nanoparticle-Based Activatable Near-Infrared Nanosensor for Protease Determination *In Vivo*. *Nano Lett.* **2009**, *9*, 4423−4415.
(45) Liu, P.; Yue, C.; Shi, B.; Gao, G.; Li, M.; Wang, B.; Ma, Y.; Cai, L. Dextran Based Sensitive Theranostic Nanoparticles for Near-Infrared Imaging and Photothermal Therapy *In Vitro*. *Chem. Commun. (Cambridge, U.K.)* **2013**, *49*, 6143−6145.

DOI: 10.1021/acsami.5b02037
ACS Appl. Mater. Interfaces 2016, 8, 15013−15023